

Modelling the hypothetical methane-leakage in a shale-gas project and the impact on groundwater quality

Michael O. Schwartz

Received: 7 July 2014 / Accepted: 27 September 2014 / Published online: 19 October 2014
© The Author(s) 2014. This article is published with open access at Springerlink.com

Abstract The hypothetical leakage of methane gas caused by fracking a 1,000-m deep Cretaceous claystone horizon at Damme, Germany, is simulated in a TOUGH-REACT reactive-transport model with 5,728 elements. A hypothetical leakage zone connects the Cretaceous horizon with a Quaternary potable-water aquifer (q1). Methane gas rises up to the q1 horizon in less than 2 days in all calculated scenarios. The simulations include the major constituents of groundwater as well as the seven most hazardous trace components that are natural constituents of groundwater (As, Cd, Cr, Ni, Pb, Se and U). The general trend is characterised by depletion of the natural hazardous components with decreasing acidity and oxygen fugacity in the relevant pH range (7–9). Nevertheless, the concentrations of elements whose dominant aqueous species are negatively charged in this pH range (Cr and Se) rise against the general trend due to desorption reactions. Slight enhancement effects are produced by the dissolution of contaminant-bearing oxides such as Cr-bearing goethite. In summary, the geological risks of a fracking operation are minor. The technical risks are more important. This is especially the case when rising methane gas gets into contact with fracking fluid that accidentally escapes through faulty well seals.

Keywords Groundwater protection · Hydrochemical modelling · Fracking · Natural gas

Introduction

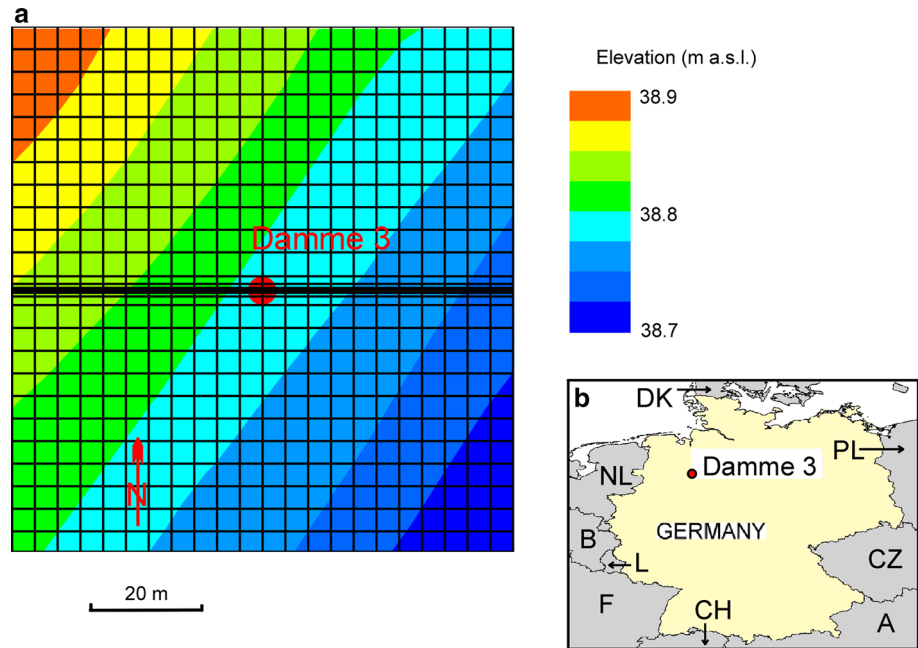
Methane is both a natural and a man-made contaminant in groundwater. Methane dissolved in drinking water is not considered to be a public health risk although medical research on this topic is limited (Jackson et al. 2011). Nevertheless, high aqueous methane concentrations affect the groundwater quality in an indirect manner. High pH together with low oxygen fugacity may cause the release of heavy metals or hazardous semi-metals from the aquifer thus posing a potential health risk.

The more evident effect of high aqueous methane concentrations is the separation of a gas phase with pressure lowering causing explosions, fires or asphyxiations. The debate on man-made methane pollution has intensified in recent years. The main reason is the increasing use of unconventional techniques in the exploitation of natural gas reservoirs. These methods are commonly based on hydraulic fracturing or fracking. The basic principle is the injection of a fracking fluid into the reservoir thus loosening the formation and releasing gas. The fluid is a mixture of water, quartz and dissolved chemicals, some of them toxic.

There is a huge amount of published information on hydraulic fracturing, the number of papers totalling 60,000 over the past 30 years (King 2012). This contrasts with the little information on hydrochemical aspects associated with the potential methane leakage during such an operation. Some papers deal with the stable isotopes of carbon, hydrogen and helium, which are meant to distinguish between man-made sources and natural occurrences (Taylor et al. 2000; Breen et al. 2007; Osborn and McIntosh 2010; Osborn et al. 2011; Stuart 2012; Jackson et al. 2013; Molofsky et al. 2013; McMahan et al. 2013). There are reports on elevated concentrations of arsenic, selenium and

M. O. Schwartz (✉)
MathGeol, Postfach 101204, 30833 Langenhagen, Germany
e-mail: mathgeol@yahoo.de

Fig. 1 TOUGHREACT model of the Damme 3 area: *Vertical nodal position* (z coordinates of the fresh water head; m a.s.l.) of the *top layer*. Location map: *A* Austria, *B* Belgium, *CH* Switzerland, *CZ* Czech Republic, *DK* Denmark, *F* France, *L* Luxembourg, *NL* Netherlands, *PL* Poland



strontium in groundwater near fracking sites in the Barnett Shale formation of north Texas but it is not known whether the contaminants have a near-surface origin or are derived from a deep source (Fontenot et al. 2013). The elevated levels of potassium, chloride and pH near fracking sites in the Wind River formation near Pavillion, Wyoming, are rather related to mixing groundwater with fracking fluid than methane intrusion (Myers 2012).

To the best of the author's knowledge, there are no descriptions of the chemical changes that are produced by methane gas escaping from the fracking zone and the movement of liquid associated with it. This paper is the first attempt to model the combined effects of intruding methane gas and aqueous liquid with respect to the mobilisation of hazardous trace elements.

The model site is the Damme area, northern Germany (Fig. 1). It is a real-world case except that a hypothetical leakage zone is included. This zone connects a deep Cretaceous horizon, which has been fracked in a pilot operation, and a shallow Quaternary aquifer, which carries potable groundwater. The site has typical features of other potential fracking targets in northern Germany (Andrulleit et al. 2012).

Materials and method

Simulation programs

The simulations are performed with a modified version of the TOUGHREACT 2.0 code, which calculates chemically

reactive flows of multi-phase fluids (Xu et al. 2012). The programme was developed by introducing reactive chemistry into the TOUGH2 flow code (Pruess et al. 1999). The governing equations are discretised using integral finite difference in space and fully implicit first-order finite difference in time.

Methane is the non-condensable gas in the modified eco2n module of the TOUGHREACT 2.0 code. Instead of calculating the three-component flow of water, NaCl and CO₂, the system water-NaCl-CH₄ is used. The thermodynamic properties of the system are identical with those of the system water-NaCl-CH₄ in the eco2 module of the TOUGHREACT 1.0 code (Xu et al. 2005). This early version of the code does not have an option for calculating surface complexation, which plays a vital role in contaminant-transport modelling.

Model site geology and hydrogeology

ExxonMobil carried out three fracs in the Damme 3 well, Lower Saxony, in 2008. To date, this the only fracking operation in a shale-gas deposit in Germany. The fracs are located at elevations of about $-1,500$, $-1,400$ and $-1,000$ m a.s.l. in the Lower Cretaceous Bückeberg formation ("Wealden facies" or "German Wealden"; Meiners et al. 2012; Sieber 2012). This limnic-brackish sequence has been deposited in the 400-km long and 100-m wide Lower Saxony basin during the Lower Cretaceous regression that effected large parts of Europe north of the Alps. The Bückeberg formation is composed of claystone, bituminous limestone, dolomitic limestone and coal seams. Its

Table 1 Set-up of the TOUGHREACT flow model

Model length/width/height (m)	88/90/1,008
General properties	
Number of elements	5,728
Number of layers	31
Simulation period (a)	1–4 days
Temperature (°C)	11.5–50
Rock grain density (kg/m ³)	2,700
Compressibility (Pa ⁻¹)	0.00
Rock grain specific heat (J/kg °C)	800
Formation heat conductivity (W/m °C)	2.1
Salinity (mass fraction NaCl)	0.00005–0.16
Diffusivity of NaCl (m ² /s)	10 ⁻⁹
Hydrogeological units	
Quaternary drift marl [q2] (thickness, m)	5.2
Quaternary sands [q1] (thickness, m)	34.8
Leakage zone (thickness, m)	968
Saturated hydraulic properties	
q2 permeability (m ²)	1 × 10 ⁻¹⁴
q1 permeability (m ²)	5 × 10 ⁻¹²
Leakage zone permeability (m ²)	1 × 10 ⁻¹⁰ –1 × 10 ⁻⁸
q2 porosity (–)	0.15
q1 porosity (–)	0.3
Leakage zone porosity (–)	0.5
Unsaturated hydraulic properties	
Residual liquid saturation (–)	0.00
Residual gas saturation	0.05
Bubbling pressure (Pa)	1.57 × 10 ⁴
Pore-size distribution index λ (–)	0.5–6.0

thickness is exceptional (>500 m) in the Damme 3 area. The 650-m thick Valanginian-Hauterivian claystone overlies the Bückeberg formation, followed by 220-m thick Upper Campanian through Eocene claystone and sandstone, 30- to 40-m thick Quaternary sands and, finally, drift marl of the Drenthe glacial stage (Table 1; Goens 2011; Gunzelmann and El Hamdaoui 2011). The freshwater head is located at about 39 m a.s.l. (Fig. 1).

The model comprises a 40-m thick Quaternary sequence of the Drenthe glacial stage with sand (q1) overlain by drift marl (q2) and a hypothetical leakage zone down to a depth of –969 m a.s.l. The vertical extension of the leakage zone is far beyond the height of a fracture that can be produced in a fracking operation. Andruleit et al. (2012) calculate that the injection of 4,400 m³ fracking fluid, such as the fluid volume for the uppermost frac in the Damme 3 well, can produce a 0.03-m wide fissure with a maximum extension of 350 m vertically and 540 m horizontally. Thus, the exceptional scenario in this paper implies the existence of a pre-fracking high-permeability zone above

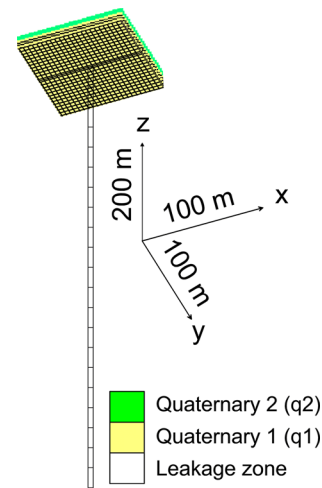


Fig. 2 Block diagram of the TOUGHREACT model of the Damme 3 area

the zone of influence of the actual fracking operation. The 0.03-m wide and 4-m long leakage zone has a permeability in the range from 10⁻¹⁰ to 10⁻⁸ m².

The justification for the exceptional scenario is the absence of published data that could characterise the integrity of the cap rock. The lack of relevant data, such as 3D seismic surveys and pre-fracking hydraulic drill-hole tests, contrasts with the wide scientific activity initiated by the Damme 3 pilot fracking test and following public debate (Sauter et al. 2012; Andruleit et al. 2012; Meiners et al. 2012; Gordalla et al. 2013; Hammes et al. 2013; Hübner et al. 2013; Kerschke and Schulz 2013; Lange et al. 2013; Olsson et al. 2013).

The already exceptional leaking-gas scenario is supplemented by an extremely pessimistic leaking-liquid scenario. It is assumed that fracking liquid leaks through faulty well seals at intermediate depths (300–350 m) and travels along subhorizontal pathways, e.g., along the Hauterivian-Campanian unconformity. The contaminated liquid is assumed to get into contact with rising methane gas. Of course, the likelihood that unfavourable geological conditions and technical failure coincide in the same operation is extremely small. Nevertheless, the wide use of the fracking technique with ten thousands of individual operations is a great challenge for the regulatory agencies. The best option is to consider even the most unlikely events.

Mesh generation

The model mesh calculated with the AMESH code (Haukwa 1998) has 31 layers with a total of 5,728 nodes and a vertical extension of 1,008 m (Figs. 1, 2; Table 1). The

topmost part of the mesh has 8 layers and a horizontal extension of 88×90 m. The remaining mesh consists of a single column with 23 elements located in the centre of the mesh below layer 8.

The eight topmost layers have a nodal distance of 4 m in the x direction and 4 sets of nodal distances in the y directions. The central segment is 0.03 m wide, followed by 0.1, 0.3 and 1 m wide segments in both y -directions. The remaining segments are 4 m wide. The top layer has nodal z values representing the freshwater head (Fig. 1). The second topmost layer has nodes located at 0.1 m below those of the top layer. The following six layers have a thickness of 5.8 m. The remaining mesh consists of a column with 22 layers with a thickness of 44 m and a bottom cell with a node located 0.1 m below that of the second lowermost cell. The horizontal dimensions of the column are identical to those of the overlying elements, i.e., a horizontal interface area of 0.12 m^2 or 4 m in the x -direction and 0.03 m in y -direction.

The top layer, which serves to maintain constant pressure (10^5 Pa), temperature and salinity, exclusively consists of infinite-volume elements (10^{52} m^3). The thermodynamic conditions of these boundary elements do not change at all. Thus, Dirichlet conditions are implemented at the boundary between the topmost and second topmost layer. The bottom cell has a volume of 10^3 m^3 . This volume is large enough for maintaining nearly constant salinity and temperature throughout the initialisation period but is simultaneously flexible enough to account for pressure adjustments. The volume of the remaining cells is calculated according to their nodal positions.

Initialisation of flow and non-reactive transport conditions

The infinite-volume elements of the top layer (10^{52} m^3), which impose Dirichlet conditions, have a pressure of 10^5 Pa and a temperature of 11.5 °C. The salinity is set at 0.00005 mass fraction NaCl, which corresponds to the median Cl concentrations of potable groundwater in northern Germany (Kringel and Bahr 2006). The large-volume element (10^3 m^3) of the bottom cell at -969 m a.s.l. imposes nearly Dirichlet conditions with respect to temperature and salinity. The temperature in this layer is 50 °C and the salinity is set at 0.16 mass fraction salt (Müller and Papendieck 1975). The intermediate layers have pre-initialisation temperature and salinity values that are interpolated according to their depths. The concentration of non-reactive tracer and the gas saturation is zero in all cells.

The initialisation is carried out in a 100-year base-case run and two sensitivity-case runs. The base-case initialisation is performed with a leakage zone having a

permeability of 10^{-8} m^2 , which is close to the theoretical maximum of 10^{-7} m^2 (Langguth and Voigt 2004). In addition, two sensitivity-case initialisations are performed with lower permeabilities (10^{-10} and 10^{-9} m^2). The saturated hydraulic properties of the two remaining geological units are identical in the base case and the sensitivity cases (Table 1). Due to the lack of site-specific information, the data from a similar study of the Gorleben area (Schwartz 2012) have been assigned to the Quaternary sands (q1) and drift marl (q2).

Flow and non-reactive transport simulation

The slightly modified output of the flow and non-reactive transport initialisation run is used as initial flow condition for the TOUGHREACT base-case simulation. The CH_4 gas saturation in the lowermost cell is changed from zero to 0.2. The concentration of the non-reactive aqueous tracer 1 and 2 is changed from zero to 0.001 mol/L in the layer 15 (-306 m a.s.l.) and layer 16 (-350 m a.s.l.), respectively. The volume of the lowermost cell is increased from 10^3 m^3 to 10^{52} m^3 ; thus perfect Dirichlet conditions are implemented at the boundary between the lowermost and second lowermost layer.

The capillary pressure and the relative permeability are calculated with the functions of Brooks and Corey (1964), which use the parameters λ (pore-size distribution index) and P_c (bubbling pressure). The base-case λ value is 2.0. The same value is incorporated in the relative-permeability function of Corey (1954). In addition, two sensitivity cases are calculated with $\lambda = 0.5$ and $\lambda = 6.0$, thus covering the full range of experimental λ values published by Brooks and Corey (1964). The P_c value, which relatively little influences the two-phase flow conditions, is that of the Apache Leach tuff reported by Rasmussen (2001) in all scenarios.

Initialisation of reactive-transport conditions

The initial solutions of the entire model are in equilibrium with the solid phases shown in Table 2 and are subject to equilibrium surface-complexation reactions with illite. The calculations are performed with an expanded THERMOCHEM thermodynamic database (Blanc et al. 2012) using all aqueous species of the elements shown in Table 3. The modification consists of adding surface complexation reactions with illite and dissociation reactions of $\text{UO}_{2.69}$ (solid phase) and galena with a Gibbs free energy of formation of -20.7 kcal/mol (Schwartz 2014). Furthermore, some new additions are necessary (Table 4 and 5):

- The solid-phase $\text{FeAs}_{0.00001}\text{Se}_{0.00001}\text{S}_{1.99998}$ (As-Se-bearing pyrite) is added. This is a calibrated phase

Table 2 Initial mineral volume fractions and kinetic properties of the TOUGHREACT transport model

Mineral	Chemical composition	Volume fraction	Reactive surface area (cm ² /g)
Quartz	SiO ₂	0.9	9.8
Illite IMt-2	K _{0.762} Na _{0.044} (Si _{3.387} Al _{0.613}) (Al _{1.427} Fe _{0.292} ⁺³ Mg _{0.241} Fe _{0.084} ⁺²)O ₁₀ (OH) ₂	0.01	151.6
Microcline	KAlSi ₃ O ₈	0.01	9.8
Siderite	FeCO ₃	0.01	9.8
Calcite	CaCO ₃	0.01	9.8
Cd-Cr-Ni-goethite	Fe _{0.999994} Cd _{0.00000001} Cr _{0.000001} Ni _{0.000005} O(OH)	0.01	12.9
UO _{2.69}	UO _{2.69}	6.4 × 10 ⁻⁷	12.9
As-Se-pyrite	FeAs _{0.00001} Se _{0.00001} S _{1.99998}	0.001	12.9
Galena	PbS	4 × 10 ⁻⁶	12.9

Mineral	Dissolution rate parameters									
	Acid mechanism				Neutral mechanism			Base mechanism		
	k ₂₅ (mol/m ² /s)	E _a (KJ/mol)	n(H ⁺)	n(Fe ⁺³)	k ₂₅ (mol/m ² /s)	E _a (KJ/mol)	n(O _{2, aq})	k ₂₅ (mol/m ² /s)	E _a (KJ/mol)	n(H ⁺)
Quartz					1.02 × 10 ⁻¹⁴	87.7				
Illite IMt-2	1.05 × 10 ⁻¹¹	23.6	0.34		1.66 × 10 ⁻¹³	35.0		3.02 × 10 ⁻¹⁷	58.9	-0.4
Microcline	8.7 × 10 ⁻¹¹	51.7	0.5		3.89 × 10 ⁻¹³	38.0		6.31 × 10 ⁻²²	94.1	-0.823
Siderite	6.5 × 10 ⁻⁴	36.1	0.5		2.95 × 10 ⁻⁸	52.2		7.76 × 10 ⁻⁶	34.8	0.5
Calcite	0.5	14.4	1.0		1.55 × 10 ⁻⁶	23.5		3.31 × 10 ⁻⁴	35.4	1.0
Cd-Cr-Ni-goethite					1.15 × 10 ⁻⁸	86.5				
UO _{2.69}					1.05 × 10 ⁻⁸	32.0				
As-Se-pyrite	3.02 × 10 ⁻⁸	56.9	-0.5	0.5	2.82 × 10 ⁻⁵	56.9	0.5			
Galena	2.34 × 10 ⁻⁷	43.5	1.0							

k₂₅ is the kinetic rate constant at 25 °C; E_a is the Arrhenius activation energy; n(H⁺) is the reaction order with respect to H⁺; n(Fe⁺³) is the reaction order with respect to Fe⁺³; n(O_{2, aq}) is the reaction order with respect to O_{2, aq}

with respect to As and Se. The dissociation constants are identical with those of pyrite.

- The solid-phase Cd_{0.00000001}Cr_{0.000001} Ni_{0.000005}-Fe_{0.999994}OOH (Cd-Cr-Ni-bearing goethite) is added. This is a calibrated phase with respect to Cd, Cr and Ni. The dissociation constants are identical with those of goethite.
- Surface-complexation reactions with adsorption of Cd and Cr onto illite are added. The equilibrium constant for Cd⁺² has been taken from Gu and Evans (2007). For Cr⁺³, the equilibrium constant for surface complexation onto hydrous ferric oxide (Scott 2010) is used.

The resulting concentrations of the trace elements in the topmost q1 layer are close to the median of the chosen reference data set. This is the hydrochemical database AQUA (Kringel and Bahr 2006), which contains the analyses of 394 samples from northern Germany, including a large range of trace elements. From these, only the trace elements are selected for this study whose median is at least 1 % of the WHO regulatory limit: As (regulatory limit

1.33 × 10⁻⁷ mol/L), Cd (2.67 × 10⁻⁸ mol/L), Cr (9.61 × 10⁻⁷ mol/L), Ni (3.41 × 10⁻⁷ mol/L), Pb (4.83 × 10⁻⁸ mol/L), Se (1.27 × 10⁻⁷ mol/L) and U (8.40 × 10⁻⁹ mol/L). As opposed to the trace components, the pH and the concentration of major elements depend on non-calibrated phases of the thermodynamic data base. Thus the initial pH and the initial concentrations of major elements in the topmost q1 layer do not necessarily have to be close to the median of the reference data set but they do lie in the range of the 10 % quantile and 90 % quantile of the reference data set (Table 3).

The surface-complexation reactions are calculated with the double-diffusive-layer model. The site density (5.8 × 10⁻⁶ mol/m²) as well as some surface-complexation equilibrium constants are taken from a compilation of Schwartz (2014), other sources being Gu and Evans (2007) and Scott (2010). The surface area for surface complexation onto illite is a calibrated maximum value. It is assumed that the maximum amount of As, Cd, Cr, Ni, Pb, Se and U adsorbed onto illite cannot be greater

Table 3 Initial water solution in the topmost layer of the q1 aquifer of the TOUGHREACT transport model and statistical parameters of the database AQUA

	TOUGHREACT model	AQUA database		
		90 % quantile	Median	10 % quantile
Temperature (°C)	11.7	12.0	10.1	8.7
pH	7.4	7.6	7.2	6.4
C (mol/L)	4.7×10^{-3}	6.1×10^{-3}	4.3×10^{-3}	1.4×10^{-3}
Cl (mol/L)	7.9×10^{-4}	2.4×10^{-3}	7.9×10^{-4}	2.8×10^{-4}
S (mol/L)	7.5×10^{-4}	1.4×10^{-3}	6.9×10^{-4}	2.3×10^{-4}
K (mol/L)	4.8×10^{-5}	1.8×10^{-4}	5.2×10^{-5}	2.8×10^{-5}
Na (mol/L)	7.4×10^{-4}	1.9×10^{-3}	7.0×10^{-4}	2.4×10^{-4}
Ca (mol/L)	1.8×10^{-3}	3.5×10^{-3}	2.4×10^{-3}	9.5×10^{-4}
Mg (mol/L)	1.3×10^{-3}	1.3×10^{-3}	5.5×10^{-4}	2.4×10^{-4}
Fe (mol/L)	3.2×10^{-5}	1.2×10^{-4}	5.7×10^{-7}	1.8×10^{-7}
Si (mol/L)	1.2×10^{-4}	3.0×10^{-4}	2.0×10^{-4}	1.2×10^{-4}
Al (mol/L)	2.5×10^{-8}	8.7×10^{-7}	7.8×10^{-8}	1.5×10^{-8}
As (mol/L)	3.5×10^{-9}	9.2×10^{-8}	2.9×10^{-9}	6.8×10^{-10}
Cd (mol/L)	3.1×10^{-10}	1.3×10^{-9}	2.8×10^{-10}	$<1.0 \times 10^{-10}$
Cr (mol/L)	1.8×10^{-8}	2.5×10^{-8}	1.3×10^{-8}	$<1.0 \times 10^{-9}$
Ni (mol/L)	2.4×10^{-8}	9.0×10^{-8}	2.3×10^{-8}	6.9×10^{-9}
Pb (mol/L)	8.2×10^{-10}	2.8×10^{-9}	7.2×10^{-10}	2.4×10^{-10}
Se (mol/L)	3.9×10^{-9}	1.2×10^{-8}	4.4×10^{-9}	1.5×10^{-9}
U (mol/L)	1.9×10^{-9}	9.8×10^{-9}	2.1×10^{-9}	9.2×10^{-11}

Table 4 Equilibrium constants [log(K)] for dissociation reactions of pollutant phases added to the THERMOTDEM thermodynamic database, used for TOUGHREACT simulations

Reaction	Equilibrium constant		
	0.01 °C	25 °C	60 °C
As-Se-bearing pyrite			
$\text{FeAs}_{0.00001}\text{Se}_{0.00001}\text{S}_{1.99998} + 3.4999725 \text{O}_{2,\text{aq}} + 1.000005 \text{H}_2\text{O} = \text{Fe}^{+2} + 1.99997 \text{H}^+ + 1.99998 \text{SO}_4^{-2} + 0.00001 \text{HSe}^- + 0.00001 \text{As}(\text{OH})_{3,\text{aq}}$	239.447	217.193	190.827
Galena			
$\text{PbS} + 2 \text{O}_{2,\text{aq}} = \text{Pb}^{+2} + \text{SO}_4^{-2}$	137.795	125.231	110.342
Cd-Cr-Ni-bearing goethite			
$\text{Fe}_{0.999994}\text{Cd}_{0.00000001}\text{Cr}_{0.000001}\text{Ni}_{0.000005}\text{O}(\text{OH}) + 2.000001 \text{H}^+ = 0.24999975 \text{O}_{2,\text{aq}} + 1.5000005 \text{H}_2\text{O} + 0.999994 \text{Fe}^{+2} + 0.00000001 \text{Cd}^{+2} + 0.000001 \text{Cr}^{+3} + 0.000005 \text{Ni}^{+2}$	-8.727	-8.128	-7.404
Uraniumoxide			
$\text{UO}_{2.69} + 2\text{H}^+ + 0.155 \text{O}_{2,\text{aq}} = \text{H}_2\text{O} + \text{UO}_2^{+2}$	13.591	11.840	9.830

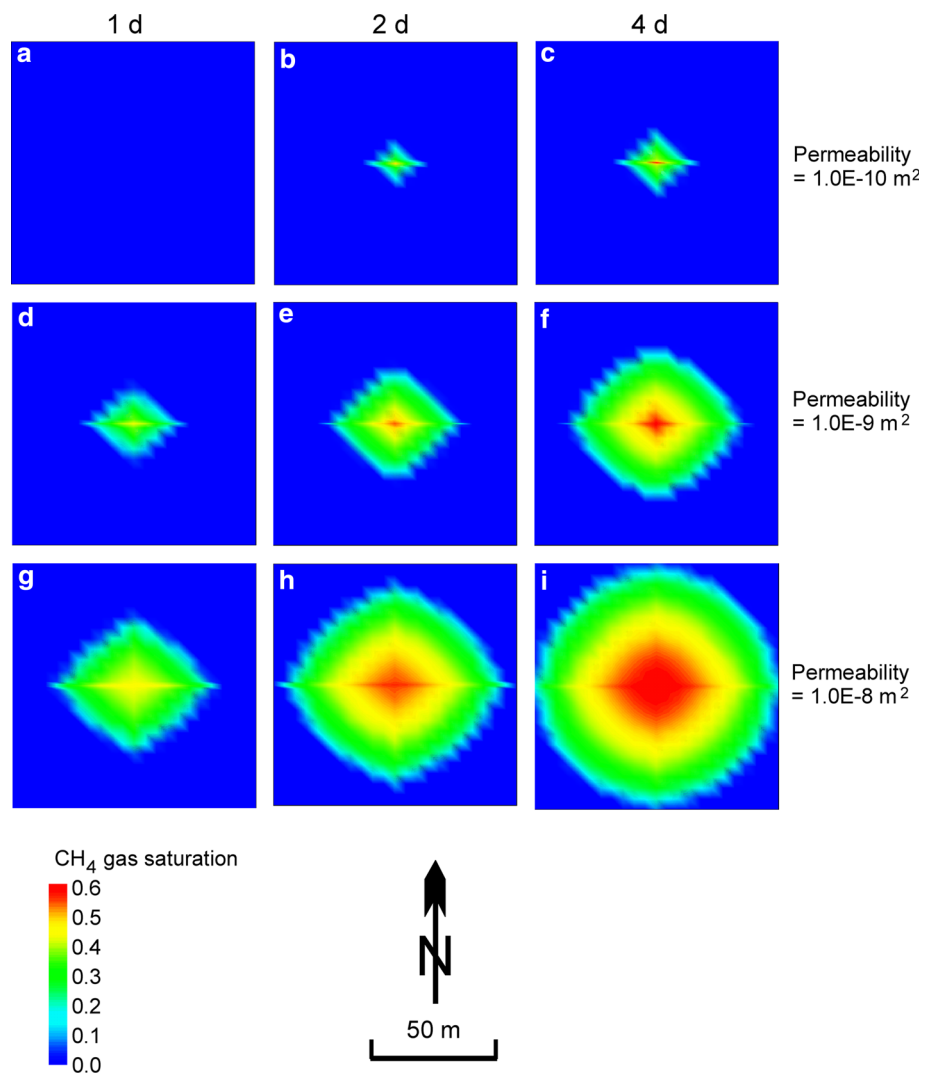
than the amounts corresponding to the average concentrations in sands and sandstone. The limit is set by the average As concentration in sandstone (1.4 ppm As; Wedepohl 1969–1978), assuming a rock grain density of 2.7 g/cm^3 . Accordingly, the maximum adsorbent surface area (base-case surface area) is $9.6 \times 10^3 \text{ cm}^2/\text{g}$, other configurations allowing a greater surface area. The reactive surface areas (Table 2), which are independent of the surface areas for surface complexation (adsorption), are based on Xu et al. (2012).

The initial fluid composition is determined with the calibrated mineral zones at temperatures and pressures calculated with the coupled flow module of TOUGHREACT. The pre-initialisation Cl concentration is $7.9 \times 10^{-4} \text{ mol/L}$ from the top of the model down to a depth of -175 m a.s.l. , and then linearly increases up to 1.8 mol/L down the model at -527 m a.s.l. but remains constant down to the bottom of the model at -969 m a.s.l. The concentrations of Na are adapted in such a manner that the charge balance is maintained.

Table 5 Equilibrium constants [log(K)] for surface-complexation reactions of the TOUGHREACT transport model

Reaction	Equilibrium constant	Source
$(I)SiH_2AsO_3 + H_2O = (I)SiOH + As(OH)_{3,aq}$	-4.490	Schwartz (2014)
$(I)SiHAsO_3^- + H_2O + H^+ = (I)SiOH + As(OH)_{3,aq}$	1.850	Schwartz (2014)
$(I)SiAsO_3^{2-} + H_2O + 2H^+ = (I)SiOH + As(OH)_{3,aq}$	11.200	Schwartz (2014)
$((I)SiO)_2Ni + 2H^+ = 2(I)SiOH + Ni^{+2}$	-0.34	Schwartz (2014)
$((I)SiO)_2Pb + 2H^+ = 2(I)SiOH + Pb^{+2}$	-1.10	Schwartz (2014)
$((I)SiO)_2Cd + 2H^+ = 2(I)SiOH + Cd^{+2}$	0.05	Gu and Evans (2007)
$(I)SiHSe + H_2O = (I)SiOH + HSe^- + H^+$	-17.50	Schwartz (2014)
$(I)SiOUO_2^+ + H^+ = (I)SiOH + UO_2^{+2}$	1.360	Schwartz (2014)
$(I)SiOUO_2OH + 2H^+ = (I)SiOH + UO_2^{+2} + H_2O$	5.320	Schwartz (2014)
$(I)SiOCrOH^+ + 2H^+ = (I)SiOH + Cr^{+3} + H_2O$	-2.06	See text

Fig. 3 TOUGHREACT 2.0 models for the Damme 3 area. CH₄ gas saturation in the top layer of the Quaternary sands (q1) for the base-case permeability of the leakage zone (10⁻⁸ m²) and sensitivity case permeabilities of the leakage zone (10⁻⁹ and 10⁻¹⁰ m²) at the end of the 1-day, 2-days and 4-days simulation periods. The pore size distribution index is 2.0 (base case)



Apart from the base case, eight sensitivity cases are calculated. The initialisation of these cases is identical to that of the base case except that some sensitivity cases use

different configurations with respect to surface complexation. The initialisation of these cases is performed with adsorption onto illite with base-case surface areas for

surface complexation multiplied with 0.1 as well as with zero adsorption.

Reactive-transport simulation

The slightly modified output of the flow initialisation run is used as initial flow condition for the TOUGHREACT base-case simulation. The modification consists of changing the CH_4 gas saturation in the lowermost cell from zero to 0.2. Another modification concerns the model mesh. The volume of the lowermost cell is increased from 10^3 m^3 to 10^{52} m^3 ; thus perfect Dirichlet conditions are implemented at the boundary between the lowermost and second lowermost layer.

Surface complexation reactions are calculated as equilibrium reactions according to the requirements of the code. In contrast, the mineral reactions are calculated as kinetically controlled reactions. The dissolution-rate parameters are taken from a compilation of Palandri and Kharaka (2004) except those for galena (Zhang et al. 2004), whereby the parameters for dolomite, smectite and uraninite are used for siderite, illite and $\text{UO}_{2.69}$, respectively (Table 2). Precipitation-rate parameters are assumed to be equal to dissolution-rate parameters. The simulation period is 1, 2 and 4 days.

For the eight sensitivity cases, the simulation procedure is identical to that of the base case except that different settings with respect to surface complexation and/or kinetically controlled reactions rates are used. The sensitivity-case rate constants are the base-case rate constants multiplied by 0.1 and 0.01. The sensitivity-case adsorption scenarios refer to base-case surface areas of illite multiplied by 0.1. Another set of sensitivity cases completely neglects adsorption.

Results

Base case

The rapid upward movement of methane gas in the leakage zone is accompanied by a much less dynamic migration of the liquid phase. At the start of the simulation, methane gas is only present in the lowermost cell at -969 m a.s.l. In little less than half a day, methane gas arrives at the third topmost layer (top of the potable water aquifer) and, after 4 days, reaches the lateral boundaries of the model (Fig. 3).

The movement of liquid, which accompanies the rises of methane gas, is relatively slow. The profiles of the tracer concentrations (Fig. 4) indicate that part of the liquid column has moved upward by about 260 m at the end of the 2-day simulation period. A similar travel length can be

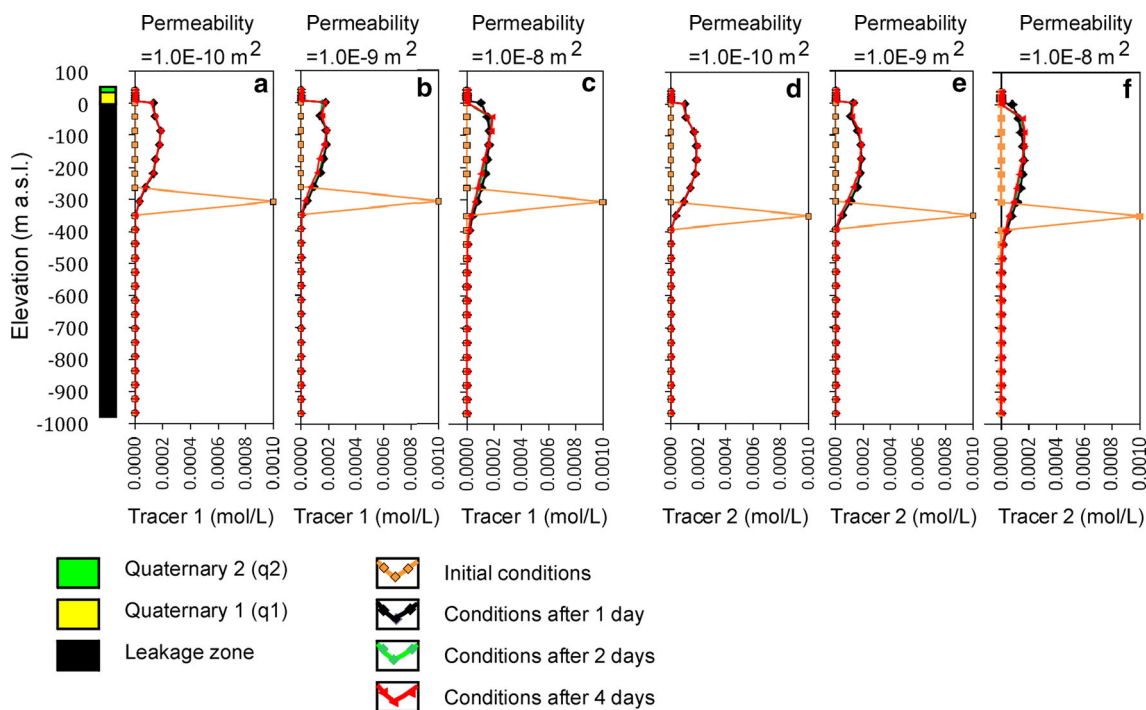


Fig. 4 TOUGHREACT 2.0 models for the Damme 3 area using the base-case permeability for the leakage zone (10^{-8} m^2) and sensitivity-case permeabilities for the leakage zone (10^{-9} and 10^{-10} m^2) in combination with the base-case pore-size distribution index of 2.0.

Concentration of the non-reactive tracer 1 and 2 in groundwater in the leakage zone and overlying layers at the beginning and end of the 1-day, 2-day and 4-day simulation periods

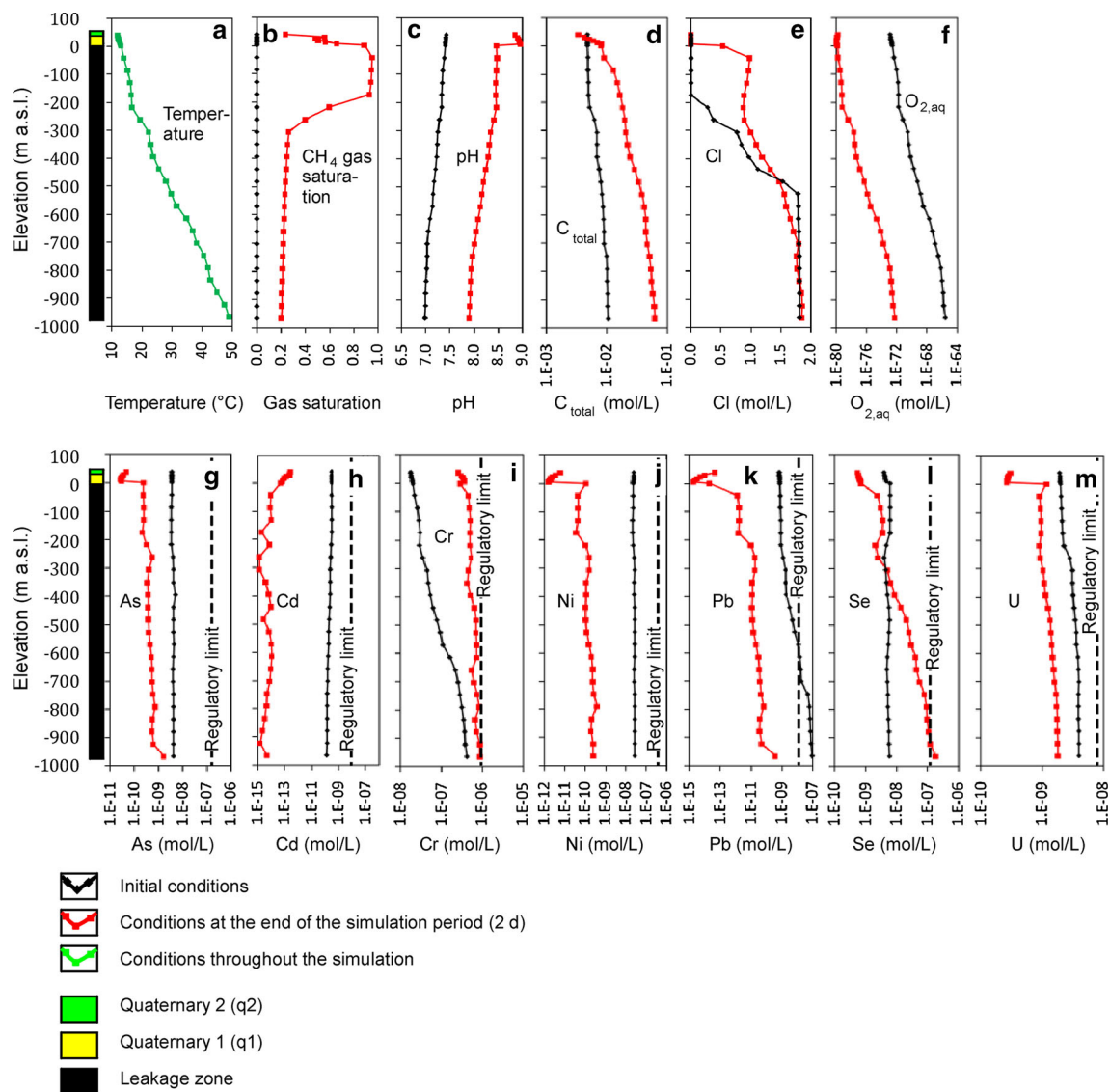


Fig. 5 TOUGHREACT 2.0 base-case model for the Damme 3 area. Temperature, CH₄ gas saturation and chemical composition of the groundwater in the vertical leakage zone and overlying layers at the beginning and end of the 2-days simulation period

deduced from the change of the Cl profile (Fig. 5). The travel length increases little if the simulation is continued beyond 4 days (not shown). This implies that rising methane gas that gets into contact with contaminated liquid (e.g. fracking fluid escaping through faulty well seals) is not capable of moving the aqueous contaminants more than 300 m vertically.

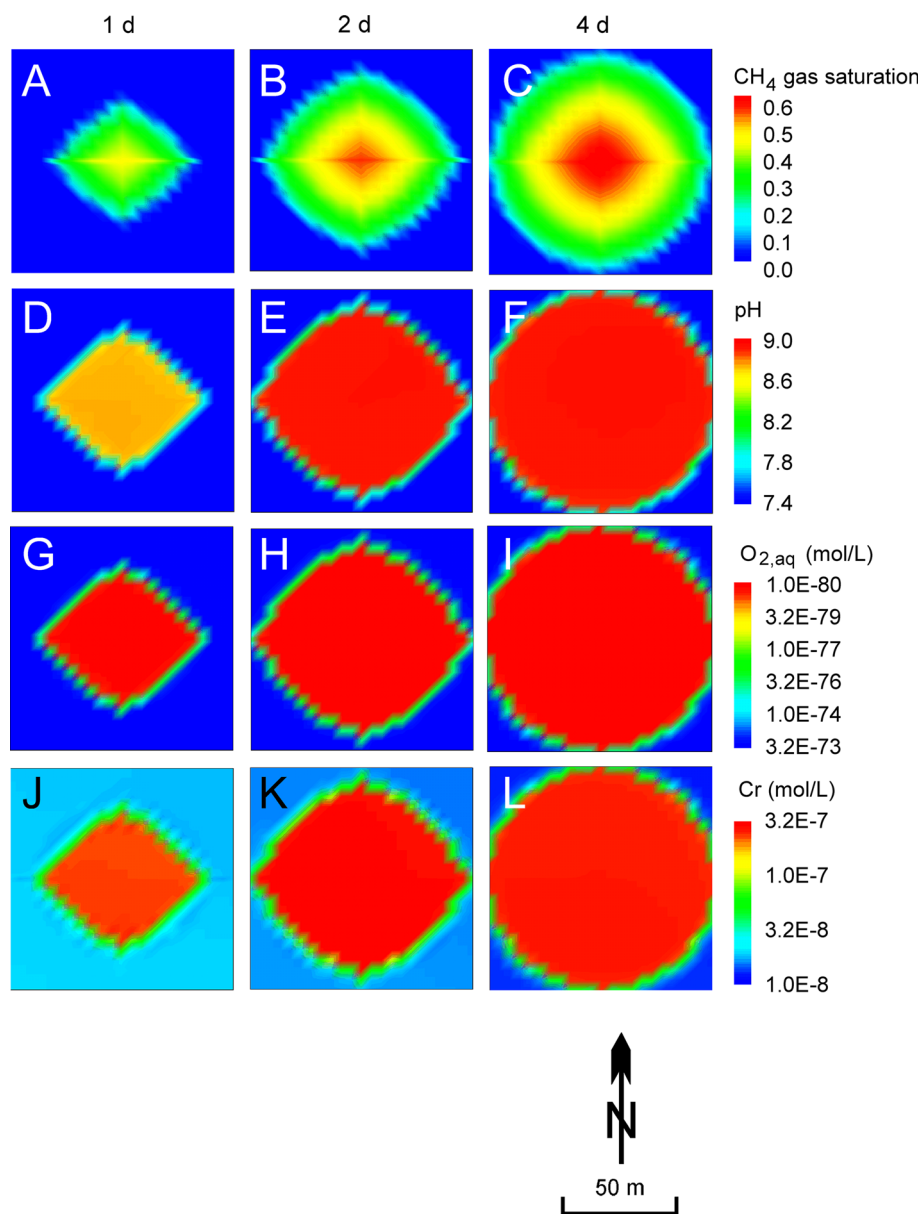
The intruding methane causes the acidity and oxygen fugacity to decrease (Figs. 6 and 7). Goethite (incorporating Cd, Cr and Ni) dissolves with decreasing acidity and oxygen fugacity whereas carbonates and sulphides (incorporating As, Cd, Pb and Se) and UO_{2.69} precipitate.

With increasing pH, the positively charged species Cd⁺², Ni⁺², Pb⁺² and UO₂⁺² as well as the neutral

aqueous species As(OH)₃ are adsorbed by surface complexation onto illite in the relevant pH range (7–9). The elements whose dominant aqueous species are negatively charged in this pH range (Cr and Se) are released with increasing pH. The desorption effect partly is counterbalanced by the precipitation of Se-bearing pyrite but enhanced by the dissolution of Cr-bearing goethite. Thus, the intrusion of methane is accompanied by a relatively strong decrease of the concentration of As, Cd, Ni, Pb and U as well as a relatively strong increase of Cr.

In the upper layer of the q1 aquifer, the distribution of the hazardous elements is mainly controlled by the distribution of methane gas, whereas in the lower layer,

Fig. 6 TOUGHREACT 2.0 base-case model for the Damme 3 area. CH₄ gas saturation, pH, concentrations of O_{2, aq} and Cr in groundwater of the top layer of the Quaternary sands (q1) at the end of the 1-day, 2-day and 4-day simulation periods



there is the additional effect of the intruding Cl-enriched aqueous phase (Fig. 5). This is only evident in the case of elements that form strong aqueous complexes with Cl (Cd, Ni and Pb). Thus, the depletion effect caused by the acidity and oxygen-fugacity decrease is only partly counterbalanced by the enhancement effect caused by the Cl component of the groundwater that accompanies the rise of methane gas. In a scenario where methane and Cl are the only additional components, the concentrations of hazardous trace components stay well below the regulatory limit except that Cr is quite close to it (9.61×10^{-7} mol/L or 50 μ g/L).

Sensitivity cases

The influence of changing flow conditions is shown by reducing the base-case permeability of the leakage zone (10^{-8} m²) by one and two orders of magnitude (Fig. 3). The low-permeability case (10^{-10} m²) implies that methane gas needs about 2 days to arrive at the top of the q1 aquifer as opposed to half a day in the high-permeability case (10^{-8} m²). The size of the plume in the low-permeability case at the end of the 4-day simulation period is smaller than that of the high-permeability case after a half-day simulation period (not shown).

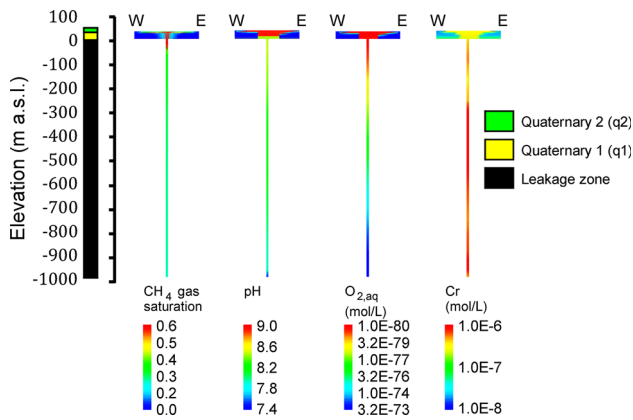


Fig. 7 TOUGHREACT 2.0 base-case model for the Damme 3 area. Vertical W–E sections with CH₄ gas saturation, pH and concentrations of O_{2,aq} and Cr in groundwater at the end of the 2-days simulation period. Horizontal exaggeration = 200 %

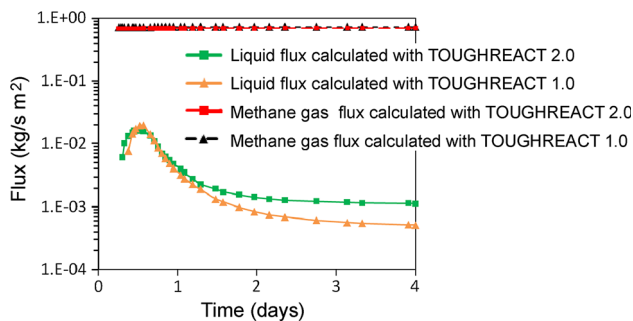


Fig. 8 Comparison of the TOUGHREACT 1.0 code and TOUGHREACT 2.0 code (modified). Simulation of the flux of liquid and methane gas at the top of the leakage zone with a permeability of 10⁻⁸ m² and pore-size distribution index of 2.0 (both are base-case values)

Figure 8 shows the flux calculations performed with the two different versions of the code, i.e. the original eco2 module of TOUGHREACT 1.0 and the modified eco2n module of TOUGHREACT 2.0 (see “Simulation programs”). The flux of methane gas at the top of the leakage zone is almost identical in both types of simulations. The flux of liquid shows some differences, which tend to decrease with decreasing permeability (not shown). Note that the differences between the two types of simulation are minor compared to the differences shown by a similar code intercomparison: the CO₂-water system modelled by the STOMP code and different versions of the TOUGH2 code with the eco2 module (Pruess et al. 2002; Fig. 4.6).

The permeability variations strongly influence the horizontal distribution of the reactive aqueous species, which correlates with the CH₄ gas saturation (not shown because a similar relationship is exhibited on the time scale; see Fig. 6). The influence of permeability variations on the

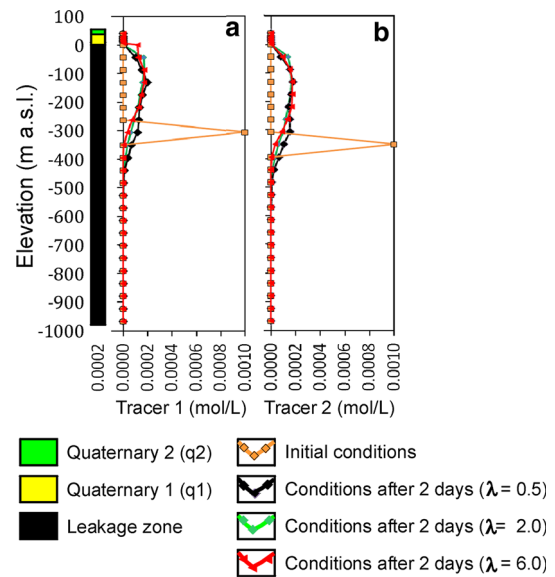


Fig. 9 TOUGHREACT 2.0 models for the Damme 3 area using the base-case pore-size distribution index ($\lambda = 2.0$) as well as sensitivity-case values of 6.0 and 0.5. The permeability of the vertical leakage zone is 10⁻⁸ m² (base case). The concentration of the non-reactive tracer 1 and 2 in groundwater in the leakage zone and overlying layers at the beginning and end of the 2-day simulation period is shown

vertical distribution of aqueous species is very minor (Fig. 4). The same goes for variations of the pore-size distribution index (Fig. 9).

The influence of changing transport conditions is shown by eight sensitivity cases, which are calculated for a simulation period of 2 days. These cases have in common that the chemical changes caused by the methane intrusion are less dynamic than those of the base case, which implies maximum values for rate constants and adsorption/desorption.

Reducing the degree of adsorption/desorption by reducing the surface area of illite or neglecting adsorption altogether reduces the degree of depletion of Ni and reduces the degree of enrichment of Cr and Se (Fig. 10). Similarly, the degree of depletion of As, Cd, Pb and U is reduced with decreasing adsorption (not shown). Note that the effect of competition for surface complexation sites is only calculated for those eight aqueous species that are defined by the reactions in Table 5. Increasing the number of competing species is theoretically possible but is hampered by the lack of suitable experimental data, in addition to convergence problems associated with such a procedure. The practical consequences are nil because increasing the degree of competition has the same effect as the reduction of the surface area of illite in the sensitivity case calculations.

Reducing the rate constants reduces the degree of depletion of Cd, Pb and Ni and reduces the degree of

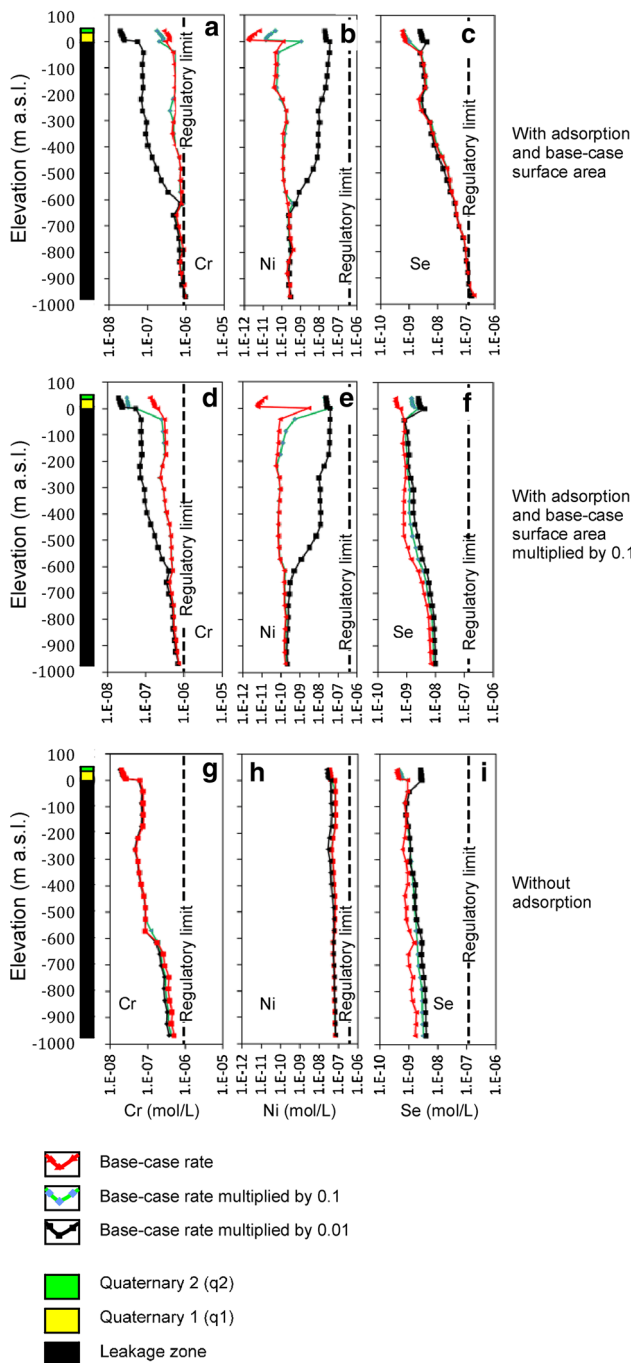


Fig. 10 TOUGHREACT 2.0 transport models for the Damme 3 area using the base-case flow model. Concentration of Cr, Ni and Se of groundwater in the vertical leakage zone and overlying layers at the end of the 2-day simulation period. **a–c** Cases with adsorption and base-case surface areas whereby the *red symbols* refer to the base case (base-case rate constant for kinetically controlled reactions) and the *green* and *black symbols* refer to sensitivity cases (base-case rate constants multiplied by 0.1 and 0.01). **d–f** Sensitivity cases with adsorption, and base-case surface areas multiplied by 0.1. **g–i** Sensitivity cases without adsorption

enrichment of Cr provided that surface complexation is considered (only shown for Cr and Ni in Fig. 10). The effects on As, Se and U concentrations are minor because the dissolution of As-Se-bearing pyrite and $\text{UO}_{2.69}$ only plays a minor role.

Discussion and conclusion

The geological risks involved in a fracking operation in methane-bearing shale are minor in comparison to the technical risks. Nevertheless, the geological hazards deserve attention. This is especially the case when methane gas risks to rise from the fracking site towards the surface. The pathway may be a fracking-induced opening, pre-existing fault zone or combination of both. Chemical reactions take place between methane, Cl-enriched groundwater and aquifer.

The methane intrusion causes the pH to increase from about 7 to 9. This is accompanied by surface complexation reactions that release elements whose dominant aqueous species are negatively charged in this pH range (Se and Cr). The desorption effect may be counterbalanced by precipitating sulphides (e.g. Se-bearing pyrite) and there may be an enhancement effect by dissolving oxides (e.g. Cr-bearing goethite). The effect of increased salinity on the distribution of elements that form strong chloride complexes (Cd, Ni and Pb) is completely offset by adsorption reactions. These are theoretical considerations. Ideally, pre-fracking hydrochemical baseline surveys and post-fracking monitoring should be combined. Short of specific studies, it is suggested that the TOUGHREACT model of this paper is used as a substitute for empirical studies. At best, this paper may stimulate combined empirical and theoretical research on sites with a hazard of methane pollution.

The unlikely case of technical failure in combination with unfavourable geological conditions would have serious consequences. The constituents of the fracking fluid impose a special risk if leakage through faulty well seals takes place less than 300 m below the potable-water aquifer. It cannot be excluded that, under unfortunate circumstances, rising methane gas gets into contact with groundwater contaminated by fracking liquid escaping through faulty well seals. Rising methane gas can induce the contaminated liquid to travel up to 300 m vertically. The sealing of the fracking wells in this particularly critical depth range, down to 300 m below the potable-water aquifer, should be optimal. Even special risk-reducing techniques such as double or triple well sealing deserve to be considered.

Open Access This article is distributed under the terms of the Creative Commons Attribution License which permits any use, distribution, and reproduction in any medium, provided the original author(s) and the source are credited.

References

- Andrulleit H, Bahr A, Bönemann C, Erbacher J, Franke D, Gerling JP, Gestermann N, Himmelsbach T, Kosinowski M, Krug S, Pierau R, Pletsch T, Rogalla U, Schlömer S (2012) Abschätzung des Erdgaspotentials aus dichten Tongesteinen (Schiefergas) in Deutschland (Estimation of the natural-gas potential in dense claystone (shale gas) in Germany). Bundesanstalt für Geowissenschaften und Rohstoffe, Germany. http://www.pebs-eu.de/DE/Themen/Energie/Downloads/BGR_Schiefergaspotenzial_in_Deutschland_2012.pdf. (Accessed 13.2.2014)
- Blanc P, Lassin A, Piantone P, Azaroual M, Jacquemet N, Fabbri A, Gaucher EC (2012) Thermodem: a geochemical database focused on low temperature water/rock interactions and waste materials. *Appl Geochem* 27:2107–2116
- Breen KJ, Révész K, Baldassare FJ, McAuley SD (2007) Natural gases in groundwater near Tioga Junction, Tioga County, North-Central Pennsylvania—occurrence and use of isotopes to determine origins, 2005. U.S. Geological Survey Scientific Investigations Report Series 2007–5085
- Brooks RH, Corey AT (1964) Hydraulic properties of porous media. Hydrology Papers 3, Colorado State University, Fort Collins, USA
- Corey AT (1954) The interrelation between gas and oil relative permeabilities. *Producer's monthly*, vol 19, no.1
- Fontenot BE, Hunt LR, Hildenbrand ZL, Carlton DD, Oka H, Walton JL, Hopkins D, Osorio A, Bjorndal B, Hu QH, Schug KA (2013) An evaluation of water quality in private drinking water wells near natural gas extraction sites in the Barnett Shale formation. *Environ Sci Technol* 47:10032–10040
- Goens J (2011) Hydrogeologische Aspekte des Fracking an der Bohrung Damme 3 (Hydrogeological aspects of fracking the well Damme 3). Landesamt für Bergbau, Energie und Geologie, Hannover, Germany. www.lbeg.niedersachsen.de/download/54607. (Accessed 13.2.2014)
- Gordalla BC, Ewers U, Frimmel FH (2013) Hydraulic fracturing: a toxicological threat for groundwater and drinking-water? *Environ Earth Sci* 70:3875–3893
- Gu X, Evans LJ (2007) Modelling the adsorption of Cd(II), Cu(II), Ni(II), Pb(II), and Zn(II) onto Fithian illite. *J Coll Inter Sci* 307:317–325
- Gunzelmann M, El Hamdaoui M (2011) Grundwassermonitoring im Bereich der Bohrungen Damme 2/3 der ExxonMobil (Groundwater monitoring for the wells Damme 2/3 of ExxonMobil). Institut Fresenius, Göttingen, Germany. http://www.damme.de/templates/images/news/1272_1.pdf. (Accessed 13.2.2014)
- Hammes U, Krause M, Mutti M (2013) Unconventional reservoir potential of the upper Permian Zechstein Group: a slope to basin sequence stratigraphic and sedimentological evaluation of carbonates and organic-rich mudrocks, Northern Germany. *Environ Earth Sci* 70:3797–3816
- Haukwa CB (1998) AMESH—a mesh creating program for the integral finite difference method. Earth Sciences Division, Lawrence Berkeley National Laboratory, Berkeley, USA
- Hübner A, Horsfield B, Kapp I (2013) Fact-based communication: the Shale Gas Information Platform SHIP. *Environ Earth Sci* 70:3921–3925
- Jackson RB, Pearson BR, Osborn SG, Warner NR, Vengosh A (2011) Research and policy recommendations for hydraulic fracturing and shale-gas extraction. Center on Global Change, Duke University, Durham, NC, U.S.A. <http://nicholas.duke.edu/cgc/HydraulicFracturingWhitepaper2011.pdf>. (Accessed 13.2.2014)
- Jackson RB, Vengosh A, Darrah TH, Warner NR, Down A, Poreda RJ, Osborn SG, Zhao KG, Karr JD (2013) Increased stray gas abundance in a subset of drinking water wells near Marcellus shale gas extraction. *PNAS* 110:11250–11255
- Kerschke DI, Schulz HM (2013) The shale gas potential of Tournaisian, Viséan, and Namurian black shales in North Germany: baseline parameters in a geological context. *Environ Earth Sci* 70:3817–3837
- King GE (2012) Hydraulic fracturing 101: What every representative, environmentalist, regulator, reporter, investor, university researcher, neighbor and engineer should know about estimating frac risk and improving frac performance in unconventional gas and oil wells. Paper prepared for presentation at the SPE Hydraulic Fracturing Technology Conference held in The Woodlands, Texas, USA, 6–8. http://fracfocus.org/sites/default/files/publications/hydraulic_fracturing_101.pdf. (Accessed 13.2.2014)
- Kringel R, Bahr A (2006) Datenbank AQUA (Database AQUA). Bundesanstalt für Geowissenschaften und Rohstoffe, Hannover
- Lange T, Sauter M, Heitfeld M, Schetelig K, Brosig K, Jahnke W, Kissinger A, Helmig R, Ebigo A, Class H (2013) Hydraulic fracturing in unconventional gas reservoirs: risks in the geological system part 1. *Environ Earth Sci* 70:3839–3853
- Langguth HR, Voigt R (2004) Hydrogeologische Methoden, 2. Auflage (Hydrogeological methods, second edition). Springer, Berlin
- McMahon PB, Thomas JC, Hunt AG (2013) Groundwater ages and mixing in the Piceance Basin natural gas province, Colorado. *Environ Sci Technol* 47:13250–13257
- Meiners HG, Denneborg M, Müller F, Bergmann A, Weber F, Dopp E, Hansen C, Schüth C (2012) Umweltauswirkungen von Fracking bei der Aufsuchung und Gewinnung von Erdgas aus unkonventionellen Lagerstätten (Environmental impact of fracking, exploration and exploitation of natural gas in unconventional deposits). Umweltbundesamt, Dessau, Germany. <https://www.umweltbundesamt.de/sites/default/files/medien/461/publikationen/4346.pdf>. (Accessed 13.2.2014)
- Molofsky LJ, Connor JA, Wylie AS, Wagner T, Farhat SK (2013) Evaluation of methane sources in groundwater in northeastern Pennsylvania. *Groundwater* 51:333–349
- Müller EP, Papendieck G (1975) Zur Verteilung, Genese und Dynamik von Tiefenwässern unter besonderer Berücksichtigung des Zechsteins (On distribution, genesis and dynamics of deep groundwater with special consideration of the Zechstein). *Zeitschrift Geologische Wissenschaften* 3:167–196
- Myers T (2012) Review of draft: investigation of groundwater contamination near Pavillion Wyoming prepared by the Environmental Protection Agency, Ada OK. Technical memorandum. http://docs.nrdc.org/energy/files/ene_12050101a.pdf
- Olsson O, Weichgrebe D, Rosenwinkel KH (2013) Hydraulic fracturing wastewater in Germany: composition, treatment, concerns. *Environ Earth Sci* 70:3895–3906
- Osborn SG, McIntosh JC (2010) Chemical and isotopic tracers of the contribution of microbial gas in Devonian organic-rich shales and reservoir sandstones, northern Appalachian Basin. *Appl Geochem* 25:456–471
- Osborn SG, Vengosh A, Warner NR, Jackson RB (2011) Methane contamination of drinking water accompanying gas-well drilling and hydraulic fracturing. *PNAS* 108:8172–8176
- Palandri JL, Kharaka YK (2004) A compilation of rate parameters of water-mineral interaction kinetics for application to geochemical modeling. U.S. Geological Survey Open File Report 2004-1068
- Pruess K, Oldenburg C, Moridis G (1999) TOUGH2 user's guide, version 2.0. Earth Sciences Division, Lawrence Berkeley National Laboratory, Berkeley, USA

- Pruess K, García J, Kovscek T, Oldenburg C, Rutqvist J, Steefel C, Xu T (2002) Intercomparison of numerical simulation codes for geologic disposal of CO₂. Earth Sciences Division, Lawrence Berkeley National Laboratory, Berkeley, USA
- Rasmussen TC (2001) Pressure wave vs. tracer velocities through unsaturated fractured rock. In: Evans DD, Nicholson TF, Rasmussen TC (eds.) Flow and transport through unsaturated fractured rock, 2nd edition. AGU Geophysical Monograph 42, AGU, Washington, pp 45–52
- Sauter M, Helmig R, Klünker J (2012) Risiken im geologischen System bei der Fracking-Technologie (Risks in the geologic system associated with the fracking technology). Wasser und Abfall 6:16–20
- Schwartz MO (2012) Modelling groundwater contamination above a nuclear waste repository at Gorleben, Germany. Hydrogeol J 20:533–546
- Schwartz MO (2014) Modelling leakage and groundwater pollution in a hypothetical CO₂ sequestration project. Int J Greenhouse Gas Control 23:72–85
- Scott AL (2010) Sensitivity analysis of uranium speciation modeling in groundwater systems with focus on mobility. Ph.D. dissertation, Graduate School of Clemson University, Clemson, USA
- Sieber D (2012) Erdgasförderung/Fracking in Deutschland (Natural gas exploitation/fracking in Germany). ExxonMobil, Hannover, Germany http://www.dgmk.de/sieber_bg_ruhr_20121116_2.pdf. (Accessed 13.2.2014)
- Stuart ME (2012) Potential groundwater impact from exploitation of shale gas in the UK. British Geological Survey Open Report OR/12/001
- Taylor SW, Lollar BS, Wassenaar LI (2000) Bacteriogenic ethane in near-surface aquifers: implications for leaking hydrocarbon well bores. Environ Sci Technol 34:4727–4732
- Wedepohl KH (1969–1978) Handbook of geochemistry. Springer, Berlin
- Xu T, Sonnenthal E, Spycher N, Pruess K (2005) TOUGHREACT user's guide: A simulation program for non-isothermal multiphase reactive transport in variably saturated geologic media. Earth Sciences Division, Lawrence Berkeley National Laboratory, Berkeley, USA
- Xu T, Spycher N, Sonnenthal E, Zheng L, Pruess K (2012) TOUGHREACT user's guide: A simulation program for non-isothermal multiphase reactive transport in variably saturated geologic media, version 2.0. Earth Sciences Division, Lawrence Berkeley National Laboratory, Berkeley, USA
- Zhang S, Li J, Wang Y, Hu G (2004) Dissolution kinetics of galena in acid NaCl solutions at 25–75 °C. Appl Geochem 19:835–841